Helicity and Polarization Gradient Optical Trapping in Evanescent Fields

Jinsheng Lu,[1] Vincent Ginis,[1,2] Soon Wei Daniel Lim,[1] and Federico Capasso[1,*]
[1]Harvard John A. Paulson School of Engineering and Applied Sciences, 9 Oxford Street, Cambridge, Massachusetts 02138, USA
[2]Data Lab and Applied Physics, Vrije Universiteit Brussel, 1050 Brussel, Belgium

(Received 29 June 2023; accepted 13 September 2023; published 6 October 2023)

Optical traps using nonconservative forces instead of conservative intensity-gradient forces expand the trap parameter space. Existing traps with nonconservative helicity-dependent forces are limited to chiral particles and fields with helicity gradients. We relax these constraints by proposing helicity and polarization gradient optical trapping of achiral particles in evanescent fields. We further propose an optical switching system in which a microsphere is trapped and optically manipulated around a microfiber using polarization gradients. Our Letter deepens the understanding of light-matter interactions in polarization gradient fields and expands the range of compatible particles and stable trapping fields.

DOI: 10.1103/PhysRevLett.131.143803

Optical trapping has wide applications in physics [1–5], chemistry [6–8], biology [9,10], and materials science [11–13]. The conventional mechanism of optical trapping uses the gradient force, which is a conservative restoring force arising from the intensity gradients of light [14]. In contrast, nonconservative forces, e.g., the scattering force, tend to push the particle away from the trapping site and are generally detrimental to optical trapping [15–19]. According to Earnshaw's theorem, 3D optical trapping using only nonconservative forces is impossible [20]. However, optical trapping using nonconservative forces is still possible in lower-dimensional (1D or 2D) cases by constraining particle motion on one or more axes [21–24].

In laser cooling and atom trapping, polarization gradient cooling using counterpropagating waves with orthogonal polarizations can exceed the Doppler limit to attain ultralow temperatures [25–28]. Such light-matter interactions in a polarization gradient field can realize interesting new classes of optomechanical effects [29–40]. Chiral particles can be trapped using counterpropagating waves with orthogonal linear polarizations, where a helicity gradient is produced even without intensity gradients [29]. The counterpropagating waves cannot have orthogonal circular polarizations, as that would produce a helicity-free polarization gradient field with strictly linear polarizations, such that chiral particles would not experience a helicity gradient and cannot be trapped. Therefore, currently, helicity gradient optical traps require light fields with helicity gradients and chiral particles [29,30,41,42].

In this Letter, we propose and numerically demonstrate helicity gradient optical trapping of achiral particles in the evanescent fields near a flat surface and around the circumference of an optical microfiber. Particles experience a helicity-dependent lateral force in evanescent fields [43–46]. Despite being nonconservative [15], this lateral optical force can act as a restoring force, enabling lateral trapping when two orthogonal linear polarizations produce a transverse helicity gradient. Furthermore, when orthogonal circular polarizations are used, despite the transverse input polarization gradient field being helicity-free, an additional helicity gradient trapping force is generated for resonant particles due to the polarization-dependent phase-shift effect [44,47]. Finally, we propose an optical switching system where we exploit this force to trap and manipulate a microsphere around a microfiber by dynamic control of polarization.

Consider an evanescent field from total internal reflection (TIR) [Fig. 1(a)]. A particle in the evanescent field experiences a lateral force F_z in the transverse direction due to the transfer of the transverse Belinfante spin momentum (BSM) P_z^S in the direction orthogonal to light propagation. Additional analysis is included in Secs. S2 and S3 in Supplemental Material [48], which includes Refs. [46,49–52]. The lateral force on a small probe particle in the evanescent field is given by [46]

$$F_z \propto P_z^S = -\frac{1}{2}\nabla_y s_x, \tag{1}$$

where s_x is the spin angular momentum (SAM) density along the propagation direction. The helicity (σ) is the projection of the SAM onto the propagation direction and is, thus, proportional to s_x ($\sigma \propto s_x$). The lateral optical force then depends on the helicity in the evanescent fields. There also exists a vertical BSM P_y^S (Fig. S1 [48]) which can generate a polarization-dependent optical force in the vertical direction to enhance, counteract, and even reverse the gradient force in the evanescent field [Eq. (S5), Fig. S3, and Sec. S4 [48]].

In our configuration, two beams with planes of incidence crossing at an angle of γ are incident on the glass-water interface, both at $\alpha = 65°$ from the interface normal (larger than the critical angle $\alpha_c = 61°$), so that they are totally internally reflected. A larger α makes the evanescent field gradient in the y direction steeper and results in a larger lateral force for trapping (Fig. S3 [48]). When the two beams have orthogonal polarizations and the same amplitude, they generate a polarization standing wave in the transverse z direction. γ determines the periodicity of the standing wave. We choose $\gamma = 20°$, which makes the polarization variation periodicity around 1.8 μm. We can use two orthogonal linear polarizations or two orthogonal circular polarizations for the beams of helicity gradient optical traps. Although the physical trapping mechanisms in these two cases are different, both configurations can achieve stable trapping.

For the first case, when orthogonal linear polarizations with the same amplitude are used, the transverse polarization distribution is described by the Jones vector:

$$\mathbf{J}(z) = \frac{1}{\sqrt{2}}(\mathbf{J}_{\mathrm{TE}}e^{-ik_z z} + \mathbf{J}_{\mathrm{TM}}e^{ik_z z}) = \frac{1}{\sqrt{2}}\begin{pmatrix} e^{-ik_z z} \\ e^{ik_z z} \end{pmatrix}, \qquad (2)$$

where $k_z = k \sin\alpha \sin(\gamma/2)$ is the transverse wave number. k is the wave number of a single beam in the incident glass medium. $\mathbf{J}_{\mathrm{TE}} = \binom{1}{0}$ and $\mathbf{J}_{\mathrm{TM}} = \binom{0}{1}$ are the transverse electric (TE) and transverse magnetic (TM) polarizations, respectively, of the two incident beams. The transverse variation of $\mathbf{J}(z)$ [Fig. 1(b)] is a great circle trajectory on the Poincaré sphere [Fig. 1(c)]. The transverse variation of the helicity is then $\sigma(z) = \sin(2k_z z)$.

Beams with orthogonal linear polarizations generate a polarization distribution in the transverse direction where the polarization cycles between linear and circular polarization [Figs. 1(b) and 1(c)]. The corresponding helicity varies periodically from positive to negative. Thus, the helicity-dependent lateral optical force also varies in sign periodically over the transverse direction, functioning as a restoring force to trap particles at multiple transverse positions. Particles are trapped in stable equilibria in the locations at which the helicity changes from positive (σ^+) to negative (σ^-), since the lateral optical force is proportional to the helicity ($F_t \propto \sigma$) [Fig. 1(b)]. In comparison, conventional optical trapping is based on an intensity gradient with particles trapped at intensity maxima due to the gradient force ($F_g \propto \nabla I$).

In the vertical y direction, the evanescent field generates a gradient force that attracts the particle to the interface. Additionally, the scattering force will push the particle along the light propagation direction (the $+x$ direction), so the particle is not trapped in the longitudinal x direction with just a single pair of TIR beams. One can use another two beams incident from the other side (the right-hand side, with propagation in the $-x$ direction) of the TIR system in Fig. 1(a) to cancel this scattering force and keep the particle fixed in the longitudinal direction as well. The particle can then be trapped in 3D within the evanescent field of the two pairs of beams (it is not against Earnshaw's theorem, since we combine both conservative and nonconservative forces [20]).

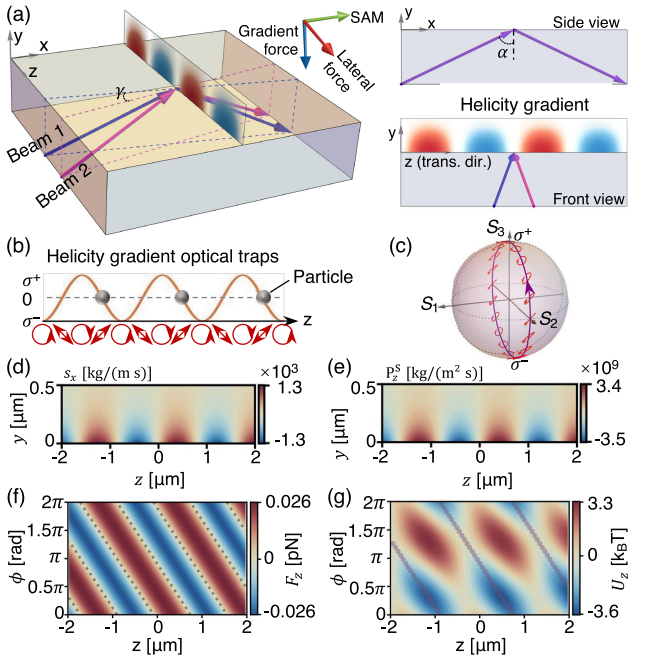

FIG. 1. Helicity gradient optical trapping of particles in a total-internal-reflection (TIR) system. (a) Two plane waves with orthogonal polarizations are incident on the glass-water interface ($y < 0$ is glass, and $y > 0$ is water) both at an angle α from the normal. The planes of incidence intersect at an angle of γ. A polarization standing wave is produced in the transverse direction with spatially varying x-directed spin angular momentum (SAM) s_x. (b) Mechanism of helicity gradient optical trapping when the two incident beams have orthogonal linear polarizations. (c) Polarization distribution in the transverse (z) direction represented on the Poincaré sphere. (d),(e) s_x (d) and transverse BSM P_z^S (e) volume density distributions in the transverse plane. (f),(g) Lateral optical force (f) and trapping potential (g) of a polystyrene particle (diameter 200 nm) along the z direction when varying the phase difference between the two beams. Black dotted lines in (f) indicate zero lateral force ($F_z = 0$). Purple dots in (g) indicate trapping positions. The unit of the trapping potential is $k_B T$, where $k_B = 1.38 \times 10^{-23}$ J · K^{-1} and $T = 293.15$ K are the Boltzmann constant and the temperature, respectively. For all simulations, $n_{\mathrm{glass}} = 1.52$, $n_{\mathrm{water}} = 1.33$, $\gamma = 20°$, $\alpha = 65°$, $\lambda = 785$ nm, and intensity $= 1$ mW/μm^2 per beam.

We perform 3D full-wave simulations of the TIR system using a commercial finite-difference time domain suite (Ansys Lumerical) to verify this theoretical model (Sec. S1 [48]). The simulated SAM s_x and BSM P_z^S volume density distributions are shown in Figs. 1(d) and 1(e), respectively. We also calculate the lateral optical force applied on a polystyrene nanoparticle with a diameter of

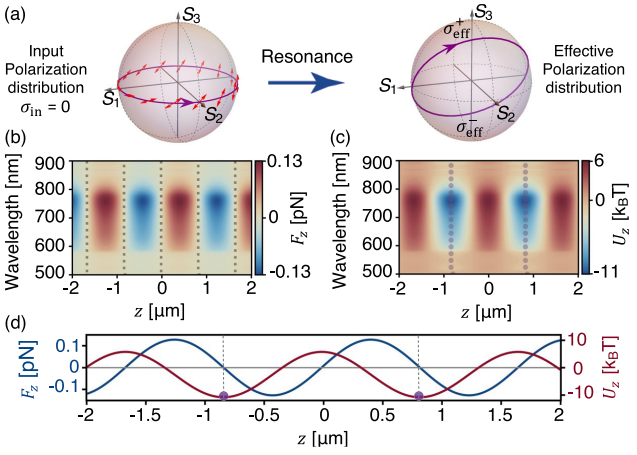

FIG. 2. Helicity gradient optical trapping in the TIR system using two orthogonal circular polarizations with identical amplitudes (intensity = 1 mW/μm^2 per beam). (a) Input and effective polarization distributions on the Poincaré sphere for a Mie particle. (b),(c) Lateral optical force (b) and trapping potential (c) of a silicon nanoparticle (diameter 200 nm) for different incident wavelengths. The nanoparticle supports electric and magnetic dipole resonances. Black dashed lines in (b) indicate $F_z = 0$. Purple dots in (c) denote stable trapping positions. (d) Lateral optical force and trapping potential at the magnetic dipole resonance wavelength (768 nm).

200 nm and a refractive index of 1.58 using the Maxwell stress tensor (Sec. S1 [48]). The results are shown in Fig. 1(f). The trapping potential U is related to the optical force F through $F = -\nabla U$. The corresponding optical trapping potential is shown in Fig. 1(g). The trapping potential depth for the polystyrene nanoparticle is $3.56\,k_BT$. As shown in Fig. 1(g), the trapping positions, indicated by the purple dots, can be tuned in the z direction by varying the phase difference ϕ between the two beams.

For the second case, when the two beams in the TIR system have orthogonal circular polarizations with the same amplitude, the polarization distribution in the transverse direction is described with the Jones vector:

$$\mathbf{J}(z) = \frac{1}{\sqrt{2}}(\mathbf{J}_{\mathrm{LCP}}e^{-ik_z z} + \mathbf{J}_{\mathrm{RCP}}e^{ik_z z}) = \begin{pmatrix} \cos(k_z z) \\ \sin(k_z z) \end{pmatrix}, \quad (3)$$

where $\mathbf{J}_{\mathrm{LCP}} = (1/\sqrt{2})\binom{1}{i}$ and $\mathbf{J}_{\mathrm{RCP}} = (1/\sqrt{2})\binom{1}{-i}$ are the left- and right-handed circular polarizations, respectively.

Orthogonal circular polarizations result in a rotating linear polarization along the lateral direction that traces the Poincaré sphere equator [the left in Fig. 2(a)]. The input field in the lateral direction has a special polarization gradient that is helicity-free [$\sigma(z) \equiv 0$], resulting in zero lateral optical force for a small particle moving in the transverse direction. Therefore, this helicity gradient optical trap does not trap small particles. However, we find this helicity gradient optical trap can still achieve trapping for a Mie particle at resonance (Sec. S5 and Fig. S4 [48]). This is because there exists a polarization-dependent phase shift ϕ_s between the TE and TM polarizations in the near field at resonance (Sec. S6 and Fig. S5 [48]). The effective polarization distribution can be described by the Jones vector:

$$\mathbf{J}_{\mathrm{eff}}(z) = \begin{pmatrix} \cos(k_z z) \\ \sin(k_z z)e^{i\phi_s} \end{pmatrix}, \quad (4)$$

which can be represented on the Poincaré sphere in the right in Fig. 2(a). The corresponding effective helicity transverse distribution is $\sigma_{\mathrm{eff}}(z) = \sin(\phi_s)\sin(2k_z z)$. This phase shift ($\phi_s$) is not limited to Mie-type resonances. Other resonances (e.g., whispering-gallery-mode resonances, to be introduced in the next section) also have this phase-shift effect [47], which contributes an additional helicity gradient for optical trapping. We call this a polarization gradient optical trap to distinguish it from the helicity gradient optical trap, since it does not use the helicity gradients of incident fields for trapping.

To show trapping in a helicity-free field, we calculate the optical force on a silicon nanoparticle (diameter = 200 nm) when the two beams have orthogonal circular polarizations. The silicon nanoparticle supports electric and magnetic dipole resonances at wavelengths of 621 and 768 nm, respectively (Fig. S4 and Sec. S5 [48]). The lateral optical force and trapping potential spectral dependencies [Figs. 2(b) and 2(c)] reach 0.13 pN and $16.6\,k_BT$ at the resonant peak wavelength of 768 nm, respectively [Fig. 2(d)]. To compare this helicity gradient optical trapping with traditional intensity-gradient trapping, we calculate the lateral trapping force of the same nanoparticle when the two beams have the same polarization, generating a lateral intensity standing wave that produces a smaller maximum trapping force of 0.09 pN.

To demonstrate the use of these polarization gradient optical traps, we propose an optical switching system based on a microfiber-microsphere configuration [Fig. 3(a)]. The input microfiber is surrounded by four output microfibers from which signal light (purple arrows) is collected. The microsphere functions as a light coupler between the input and output fibers when it is trapped between them. The azimuthal trapping position of the microsphere is dynamically controlled by the control light polarization (red arrows), allowing it to behave as a light switch (Supplemental Video [48]). We use two counterpropagating light beams in the input fiber as control light to cancel out the scattering force in the axial direction. The control light has a fiber mode ($\mathrm{HE}_{11}^{y} + \mathrm{HE}_{11}^{z}e^{i\phi}$) which is a combination of two fundamental polarization-orthogonal fiber modes HE_{11}^{y} and HE_{11}^{z} with a phase difference ϕ between them. ϕ determines the control light polarization, yielding RCP, LCP, and ±45° diagonal polarizations when $\phi = \pi/2$, $-\pi/2$, 0, and π, respectively.

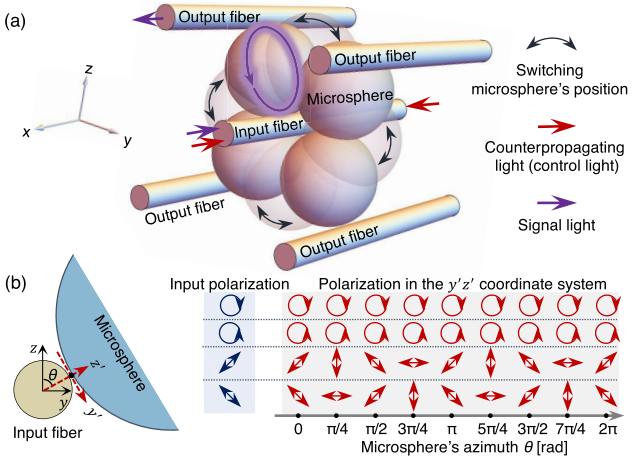

FIG. 3. Polarization gradient optical trapping in a microfiber-microsphere system for optical switching. (a) Schematic of an optical switching system. One input microfiber is surrounded by four output microfibers. The purple circle indicates a whispering-gallery mode. See the Supplemental Video [48] for a more detailed demonstration of the optical switching system. (b) Polarizations in the $y'z'$ coordinate system at different azimuth positions. The lateral direction is along the y' direction tangent to the input fiber. The input fiber and the microsphere are represented by the yellow circle and the blue partial circle, respectively. Four input polarizations (the polarization of the control light in the input fiber) are considered: RCP, LCP, and $\pm 45°$ diagonal polarizations. The polarization state in the $y'z'$ coordinate system varies with the microsphere's azimuthal position when the input polarization is noncircular.

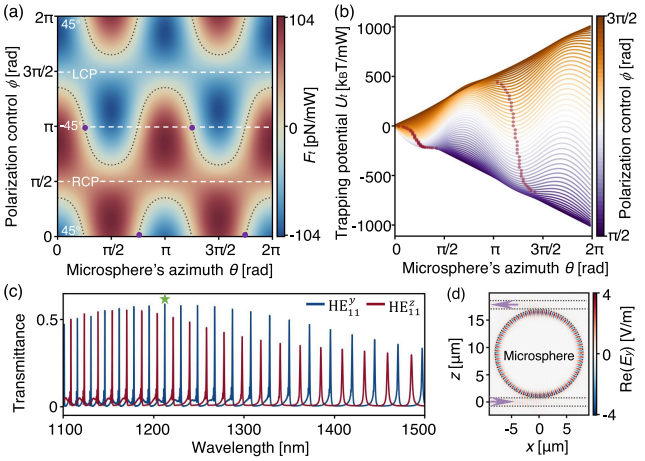

FIG. 4. Simulation of polarization gradient optical trapping in the microfiber-microsphere system. (a),(b) Lateral optical force F_t on the microsphere (a) and trapping potential (b) at different azimuthal positions when varying the control light polarization. The black dashed curves in (a) are the contour lines for $F_t = 0$. The four purple dots indicate trapping sites when input linear polarizations are diagonal ($\pm 45°$). Red dots in (b) indicate local potential minima (trapping sites). The microfiber and microsphere radii are 0.8 and 8.0 μm, respectively. The control light wavelength is 1408.6 nm. (c) The transmission spectrum at the output fiber when the microsphere is in a trapping state. (d) Electric field distribution in the xz cross section at $\lambda = 1212.5$ nm, the peak transmittance wavelength [green star in (c)].

Next, we explain the origin of the polarization gradient and present the physical mechanism of microsphere optical trapping in the input fiber's azimuthal direction. We consider a new $y'z'$ coordinate system [red dashed arrows in Fig. 3(b)] which is obtained by rotating the yz coordinate system [black arrows in Fig. 3(b)] with an angle of θ. θ indicates the microsphere's azimuth around the input fiber. The optical lateral force F_t on the microsphere is along the y' direction (tangential to the input fiber). The input fiber polarization in the yz and $y'z'$ coordinate systems is $\mathbf{J}_0$ and $\mathbf{J}'$, respectively. We can obtain $\mathbf{J}'(\theta)$ by performing a rotational transform of the input polarization $\mathbf{J}_0$: $\mathbf{J}'(\theta) = R(-\theta)\mathbf{J}_0$, where $R(-\theta) = \begin{pmatrix} \cos\theta & \sin\theta \\ -\sin\theta & \cos\theta \end{pmatrix}$ is the clockwise rotation matrix.

When the input polarization is circular [$\mathbf{J}_0 = (1/\sqrt{2})\binom{1}{\pm i}$], the polarization in the $y'z'$ coordinate system is circular for any azimuth θ: $\mathbf{J}'(\theta) = (1/\sqrt{2})e^{-i\theta}\binom{1}{\pm i}$, as shown in Fig. 3(b). The polarization-dependent lateral optical force remains the same when the microsphere moves to different positions around the microfiber [white dashed lines "RCP" or "LCP" in Fig. 4(a)], enabling an orbiting motion. When the input polarization $\mathbf{J}_0$ is not circular, for example, $\pm 45°$ diagonal [$\mathbf{J}_0 = (1/\sqrt{2})\binom{1}{\pm 1}$], the polarization in the $y'z'$ coordinate system is given by

$$\mathbf{J}(\theta) = \frac{1}{\sqrt{2}}\begin{pmatrix} \cos\left(-\theta \pm \frac{\pi}{4}\right) \\ \sin\left(-\theta \pm \frac{\pi}{4}\right) \end{pmatrix}, \tag{5}$$

which varies with the azimuth θ, presenting a polarization gradient in the azimuthal direction [Fig. 3(b)]. This polarization gradient is similar to that of the TIR system with orthogonal circular polarizations [Fig. 2]. An effective helicity gradient is generated at microsphere resonance, allowing it to behave as if it were in a helicity gradient optical trap in the azimuthal direction.

The lateral force of the microsphere [Fig. 4(a)] yields the azimuthal trapping potential around the microfiber [Fig. 4(b)]. The microsphere will be trapped in azimuthal positions with local trapping potential minima, which can be controlled by changing the input polarization [red dots are trapping sites in Fig. 4(b)]. The trapping position can be tuned to almost any azimuthal position (except the four local regions in these azimuths $\theta = 0$, $\pi/2$, π, and $3\pi/2$), among which there are four most stable trapping local regions near $\theta = \pi/4, 3\pi/4, 5\pi/4$, and $7\pi/4$ [purple dots in Fig. 4(a)]. When $\phi = \pi/2$ ($\phi = 3\pi/2$), the microsphere performs orbital rotation around the microfiber clockwise (counterclockwise). The trapping and orbiting behavior as a function of the polarization control phase ϕ is summarized in the Supplemental Video [48].

We further investigate the coupling efficiency of the signal light from the input fiber to the output fiber through the microsphere. The transmittance spectrum of the signal light in optical switching is shown in Fig. 4(c). Figure 4(d) highlights the electric field distribution in this structure at the resonance wavelength of 1212.5 nm. The coupling efficiency from the input fiber to the output fiber reaches 59%.

In conclusion, we demonstrate the helicity gradient optical trapping of achiral particles in evanescent fields. The principle is generalizable to any system in which evanescent fields exhibit polarization and helicity gradients. Beyond planar TIR systems, fiber-based systems with curved interfaces are also suitable compact deployment platforms [53,54]. Furthermore, propagating waves in free space can be superimposed to approximate evanescent field characteristics through superoscillations [55,56]. Wave-front-shaping devices like metasurfaces have also been used to realize large phase, polarization, and intensity gradients [33,57], suggesting that the formalism introduced here may be extended to propagating optical fields as well. This new mechanism opens a new front for light-matter manipulation in optomechanics, potentially offering extensive applications in integrated photonic systems [58–62].

We acknowledge support from the Research Foundation Flanders under Grants No. G032822N and No. G0K9322N. S. W. D. L. is supported by A*STAR Singapore through the National Science Scholarship Scheme.

*capasso@seas.harvard.edu

[1] A. Ashkin, Proc. Natl. Acad. Sci. U.S.A. **94**, 4853 (1997).
[2] R. W. Bowman and M. J. Padgett, Rep. Prog. Phys. **76**, 026401 (2013).
[3] R. J. Niffenegger, J. Stuart, C. Sorace-Agaskar, D. Kharas, S. Bramhavar, C. D. Bruzewicz, W. Loh, R. T. Maxson, R. McConnell, D. Reens *et al.*, Nature (London) **586**, 538 (2020).
[4] T. L.. Gustavson, A. P. Chikkatur, A. E. Leanhardt, A. Görlitz, S. Gupta, D. E. Pritchard, and W. Ketterle, Phys. Rev. Lett. **88**, 020401 (2001).
[5] S. Yu, J. Lu, V. Ginis, S. Kheifets, S. W. D. Lim, M. Qiu, T. Gu, J. Hu, and F. Capasso, Optica **8**, 409 (2021).
[6] P. O. Heidarsson and C. Cecconi, Essays Biochem. **65**, 129 (2021).
[7] M. Riccardi and O. J. Martin, Chem. Rev. **123**, 1680 (2023).
[8] N. Calander and M. Willander, Phys. Rev. Lett. **89**, 143603 (2002).
[9] A. Ashkin and J. M. Dziedzic, Science **235**, 1517 (1987).
[10] I. Heller, T. P. Hoekstra, G. A. King, E. J. Peterman, and G. J. Wuite, Chem. Rev. **114**, 3087 (2014).
[11] F. Ritort, S. Mihardja, S. B. Smith, and C. Bustamante, Phys. Rev. Lett. **96**, 118301 (2006).
[12] S. Burchesky, L. Anderegg, Y. Bao, S. S. Yu, E. Chae, W. Ketterle, K.-K. Ni, and J. M. Doyle, Phys. Rev. Lett. **127**, 123202 (2021).
[13] Z. Yan, M. Sajjan, and N. F. Scherer, Phys. Rev. Lett. **114**, 143901 (2015).
[14] A. Ashkin, J. M. Dziedzic, J. E. Bjorkholm, and S. Chu, Opt. Lett. **11**, 288 (1986).
[15] S. Sukhov and A. Dogariu, Rep. Prog. Phys. **80**, 112001 (2017).
[16] A. Ashkin, Phys. Rev. Lett. **24**, 156 (1970).
[17] K. Svoboda and S. M. Block, Opt. Lett. **19**, 930 (1994).
[18] C. Min, Z. Shen, J. Shen, Y. Zhang, H. Fang, G. Yuan, L. Du, S. Zhu, T. Lei, and X. Yuan, Nat. Commun. **4**, 2891 (2013).
[19] G. Schnoering, L. V. Poulikakos, Y. Rosales-Cabara, A. Canaguier-Durand, D. J. Norris, and C. Genet, Phys. Rev. Lett. **121**, 023902 (2018).
[20] A. Ashkin and J. P. Gordon, Opt. Lett. **8**, 511 (1983).
[21] Y. Roichman, B. Sun, Y. Roichman, J. Amato-Grill, and D. G. Grier, Phys. Rev. Lett. **100**, 013602 (2008).
[22] I. Liberal, I. Ederra, R. Gonzalo, and R. W. Ziolkowski, Phys. Rev. A **87**, 063807 (2013).
[23] M. A. Zaman, P. Padhy, and L. Hesselink, Sci. Rep. **9**, 649 (2019).
[24] F. Nan, X. Li, S. Zhang, J. Ng, and Z. Yan, Sci. Adv. **8**, eadd6664 (2022).
[25] P. D. Lett, R. N. Watts, C. I. Westbrook, W. D. Phillips, P. L. Gould, and H. J. Metcalf, Phys. Rev. Lett. **61**, 169 (1988).
[26] J. Dalibard and C. Cohen-Tannoudji, J. Opt. Soc. Am. B **6**, 2023 (1989).
[27] C. N. Cohen-Tannoudji and W. D. Phillips, Phys. Today **43**, No. 10, 33 (1990).
[28] A. Dareau, Y. Meng, P. Schneeweiss, and A. Rauschenbeutel, Phys. Rev. Lett. **121**, 253603 (2018).
[29] H. Zheng, H. Chen, J. Ng, and Z. Lin, Phys. Rev. B **103**, 035103 (2021).
[30] J. Yamanishi, H.-Y. Ahn, H. Yamane, S. Hashiyada, H. Ishihara, K. T. Nam, and H. Okamoto, Sci. Adv. **8**, eabq2604 (2022).
[31] Z. He and G. Dong, J. Opt. Soc. Am. B **38**, 60 (2021).
[32] S. Albaladejo, M. I. Marqués, M. Laroche, and J. J. Sáenz, Phys. Rev. Lett. **102**, 113602 (2009).
[33] S. W. D. Lim, J.-S. Park, M. L. Meretska, A. H. Dorrah, and F. Capasso, Nat. Commun. **12**, 4190 (2021).
[34] G. Cipparrone, I. Ricardez-Vargas, P. Pagliusi, and C. Provenzano, Opt. Express **18**, 6008 (2010).
[35] JM. Nichols, DV. Nickel, and F. Bucholtz, Opt. Express **30**, 38907 (2022).
[36] L. Cai, S. Zhang, W. Zhu, H. Wu, H. Zheng, J. Yu, Y. Zhong, and Z. Chen, Opt. Lett. **45**, 6740 (2020).
[37] L. Wei and F. J. Rodríguez-Fortuño, Phys. Rev. B **105**, 125424 (2022).
[38] N. Kravets, A. Aleksanyan, and E. Brasselet, Phys. Rev. Lett. **122**, 024301 (2019).
[39] T. Zhang, M. R. C. Mahdy, Y. Liu, J. H. Teng, C. T. Lim, Z. Wang, and C.-W. Qiu, ACS Nano **11**, 4292 (2017).
[40] M. Nieto-Vesperinas, Phys. Rev. A **92**, 043843 (2015).
[41] L. Fang and J. Wang, Phys. Rev. Lett. **127**, 233902 (2021).
[42] Y. Liu, W. Zhang, L. He, and X. Zhang, APL Photonics **8**, 036112 (2023).
[43] L. Liu, A. Di Donato, V. Ginis, S. Kheifets, A. Amirzhan, and F. Capasso, Phys. Rev. Lett. **120**, 223901 (2018).

[44] V. Ginis, L. Liu, A. She, and F. Capasso, Sci. Rep. **9**, 14879 (2019).
[45] A. Hayat, J. B. Mueller, and F. Capasso, Proc. Natl. Acad. Sci. U.S.A. **112**, 13190 (2015).
[46] K. Y. Bliokh, A. Y. Bekshaev, and F. Nori, Nat. Commun. **5**, 3300 (2014).
[47] J. Lu, V. Ginis, C.-W. Qiu, and F. Capasso, Phys. Rev. Lett. **130**, 183601 (2023).
[48] See Supplemental Material at http://link.aps.org/supplemental/10.1103/PhysRevLett.131.143803 for numerical simulation method, lateral optical force and Belinfante spin momentum, analytical calculations of optical forces on dipole particles, repulsive force in evanescent fields, multipole decomposition of Mie-resonance particles, resonance-induced phase-shift effect, and the influence of the misalignment of two beams in the TIR system.
[49] L. Novotny and B. Hecht, *Principles of Nano-Optics* (Cambridge University Press, Cambridge, England, 2012).
[50] A. Y. Bekshaev, J. Opt. **15**, 044004 (2013).
[51] A. Y. Bekshaev, J. Opt. **18**, 029501 (2016).
[52] D. Sikdar, W. Cheng, and M. Premaratne, J. Appl. Phys. **117**, 083101 (2015).
[53] J. Lu, H. Yang, L. Zhou, Y. Yang, S. Luo, Q. Li, and M. Qiu, Phys. Rev. Lett. **118**, 043601 (2017).
[54] J. Lu, Q. Li, C.-W. Qiu, Y. Hong, P. Ghosh, and M. Qiu, Sci. Adv. **5**, eaau8271 (2019).
[55] G. Yuan, E. T. F. Rogers, and N. I. Zheludev, Light **8**, 2 (2019).
[56] C. M. Spägele, M. Tamagnone, S. W. D. Lim, M. Ossiander, M. L. Meretska, and F. Capasso, Sci. Adv. **9**, eadh0369 (2023).
[57] S. W. D. Lim, J.-S. Park, D. Kazakov, C. M. Spägele, A. H. Dorrah, M. L. Meretska, and F. Capasso, Nat. Commun. **14**, 3237 (2023).
[58] L. Fang and J. Wang, Opt. Lett. **46**, 2316 (2021).
[59] L. Fang, H.-Z. Luo, X.-P. Cao, S. Zheng, X.-L. Cai, and J. Wang, Optica **6**, 61 (2019).
[60] V. Ginis, I.-C. Benea-Chelmus, J. Lu, M. Piccardo, and F. Capasso, Nat. Commun. **14**, 495 (2023).
[61] S. Linghu, Z. Gu, J. Lu, W. Fang, Z. Yang, H. Yu, Z. Li, R. Zhu, J. Peng, Q. Zhan *et al.*, Nat. Commun. **12**, 385 (2021).
[62] Q. Jia, W. Lyu, W. Yan, W. Tang, J. Lu, and M. Qiu, Photonics Insights **2**, R05 (2023).